Landmark Constrained Genus-one Surface Teichmüller Map Applied to Surface Registration in Medical Imaging

Ka Chun Lam[a], Xianfeng Gu[b], Lok Ming Lui[a,*]

[a]*Department of Mathematics, The Chinese University of Hong Kong, Shatin, Hong Kong*
[b]*Department of Computer Sciences, Stony Brook University*

Abstract

We address the registration problem of genus-one surfaces (such as vertebrae bones) with prescribed landmark constraints. The high-genus topology of the surfaces makes it challenging to obtain a unique and bijective surface mapping that matches landmarks consistently. This work proposes to tackle this registration problem using a special class of quasi-conformal maps called Teichmüller maps (T-Maps). A landmark constrained T-Map is the unique mapping between genus-1 surfaces that minimizes the maximal conformality distortion while matching the prescribed feature landmarks. Existence and uniqueness of the landmark constrained T-Map are theoretically guaranteed. This work presents an iterative algorithm to compute the T-Map. The main idea is to represent the set of diffeomorphism using the Beltrami coefficients(BC). The BC is iteratively adjusted to an optimal one, which corresponds to our desired T-Map that matches the prescribed landmarks and satisfies the periodic boundary condition on the universal covering space. Numerical experiments demonstrate the effectiveness of our proposed algorithm. The method has also been applied to register vertebrae bones with prescribed landmark points and curves, which gives accurate surface registrations.

Keywords: Surface Registration, genus-one, Teichmuller map, Beltrami coefficient, landmark, vertebrae bones

1. Introduction

Surface-based morphometry of human anatomical structures has received much attention recently for disease analysis (Drury et al., 1996; Fischl et al., 1999a,b; Thompson et al., 2000; Vaillant et al., 2007; Chung et al., 2003, 2008; Lui et al., 2010b, 2012; Zhang et al., 2012). For example, surface-based shape analysis has been extensively applied for examining brain cortical (Thompson et al., 2000; Vaillant et al., 2007; Chung et al., 2003, 2008) and sub-cortical structures (Lui et al., 2010b, 2012; Zhang et al., 2012; Wong et al., 2012) to analyze diseases such as Alzheimer's disease (Wang et al., 2009; Lui et al., 2010b) and William Syndrome (Thompson et al., 2005; Van Essen et al., 2006). In order to carry out surface-based morphometry, accurate surface registrations between corresponding structures of different subjects are necessary. By finding a meaning one-to-one vertex-wise correspondence between anatomical surfaces, various statistical shape analysis (Chung et al., 2001; Lui et al., 2010b; Wang et al., 2010) and surface processing models (Lui et al., 2013; Lam et al., 2014b) can be developed.

Due to its importance, a multitude of surface registration techniques have been recently proposed. Existing registration algorithms can mainly be divided into three categories. They are, namely, 1. Landmark-guided surface registration; 2. Geometry-guided surface registration and 3. Hybrid surface registration. Landmark-guided surface registration algorithms drive surfaces into vertex-wise correspondence based on salient features, called landmarks, defined on each surfaces. Feature landmarks can often be extracted on anatomical structures, which provide important information to drive for a good registration. For example, sulci or gyri curves on brain cortical surfaces are important anatomical features for neuroscientists to analyze brain diseases (Lui et al., 2007, 2010a) . Various algorithms have been recently developed to obtain landmark-matching surface registrations (Bookstein, 1989; Wang et al., 2005; Lui et al., 2007, 2010a; Tosun et al., 2004; Joshi and Miller, 2000; Glaunès et al., 2004). Another category of sur-

*Corresponding author
Email addresses: kclam@math.cuhk.edu.hk (Ka Chun Lam), gu@cs.stonybrook.edu (Xianfeng Gu), lmlui@math.cuhk.edu.hk (Lok Ming Lui)

face registration techniques is the geometry-guided registration algorithm. Surface registration is obtained by matching geometric quantities defined on each surfaces. Some commonly chosen geometric quantities are surface curvatures (Yeo et al., 2010), surface metric (Lord et al., 2007) , angular structure (Haker et al., 2000; Gu et al., 2004; Jin et al., 2008; Hurdal and Stephenson, 2009) and convexity (Fischl et al., 1999b). The third category of registration models is the hybrid surface registration algorithm, which combines both landmark-guided and geometry-guided registration together. Optimization approaches have been developed to compute an optimal surface mapping that matches corresponding landmarks and geometric quantities as much as possible (Johnson and Christensen, 2002; Lam and Lui, 2014).

This work mainly focuses on the landmark-based surface registration between genus-one closed surfaces (such as vertebrae bones). Landmark-guided registration is often more preferable in medical research since expert knowledge can be incorporated into the registration model. Through labeling landmarks, medical doctors and experts can get involved in the registration process to assure good correspondences between the surfaces. Registration problems for simply-connected surfaces have been well-studied. For high-genus surfaces, the surface registration becomes much more challenging because of their complicated topologies. For example, the vertebral shape is commonly analyzed through simple geometric measurements of dimensions, which only describe a limited features of the complex vertebral shape. In order to provide a more comprehensive description, a more sophisticated landmark-based surface registration is essential for analyzing both local and global geometric information of a vertebral shape. Some works have been reported recently to handle the registration problem of high-genus surfaces. In (Zhang et al., 2014), the authors proposed to cut the high-genus surfaces into simply-connected patches, and the registration can be obtained using a patch-by-patch manner. This method requires the delineation of consistent cuts, which are sometimes difficult to obtain. In (Lui and Wen, 2014), the authors proposed to embed the high-genus surfaces to the universal covering space $\mathbb{H}$ in $\mathbb{R}^2$, and carry out the registration process in $\mathbb{H}$. The algorithm computes surface registration between high-genus surfaces that matches surface curvatures. The proposed method does not require the extraction of consistent cuts. However, it is parameter dependent and cannot give a unique optimizer. The algorithm can easily get trapped at a local minimum.

On the contrary, a good surface registration model for high-genus surfaces should satisfy the following criteria:

1. **Local geometry preserving:** the geometry of a local region should be preserved after the transformation by the surface registration.
2. **Diffeomorphic:** the surface registration should be smooth and bijective (folding-free), which describes the deformation of an anatomical structure.
3. **Uniqueness:** the algorithm should give a unique solution satisfying the conditions of the registration model.
4. **Inverse consistency:** the forward and backward registrations should be inversely consistent so that the registration result is independent of the choice of source and target surfaces.
5. **Parameter independent:** ideally, the registration model should be free of parameters to avoid the hassle of finding the optimal set of parameters.
6. **Stable under landmark selection:** the algorithm should be stable under landmark selection errors.
7. **Stable under geometric noises:** geometric noises should not induce serious mis-registration.

This paper presents a novel algorithm to obtain landmark-based genus-one surface registrations via a special class of quasi-conformal maps called the Teichmuller maps, which fulfils the above seven criteria. A landmark-matching Teichmuller map between two genus-one surfaces is the unique bijective surface map that minimizes the conformality distortion. As suggested by (Thompson, 1942), conformal transformations provide the most natural way to describe the deformation or growth of biological structures. Hence, T-Maps are suitable for the surface registration of anatomical structures. Given a prescribed set of corresponding landmarks (points and/or curves) defined on each surface, the existence and uniqueness of the Teichmüller map are theoretically guaranteed. In this paper, we propose an iterative algorithm to compute the unique Teichmüller map of genus-one surfaces by adjusting the conformality measurement, called the Beltrami differential. The iterative algorithm aims to search for an optimal Beltrami differential minimizing the supreme norm subject to the landmark constraints. To facilitate the optimization process, each surface is firstly embedded in the Euclidean plane through introducing boundary cuts. Nevertheless, the algorithm is invariant to the chosen boundary cuts since the cuts are allowed to move freely on the target surface. Besides, the proposed algorithm

is parameter-free. By controlling the Beltrami differential, a diffeomorphic (folding-free) surface mapping can be guaranteed. Numerical experiments also demonstrate the proposed algorithm satisfies the inverse consistency constraints and is stable under geometry noises. Therefore, our proposed model can produce a landmark constrained genus-one surface mapping, which satisfies the abovementioned seven criteria of being a good surface registration.

The contributions of this work are two-fold. First, we introduce the landmark-matching Teichmüller map to the field of medical imaging for genus-one surface registration. Second, we propose a method to compute landmark-based Teichmüller maps of genus-one surfaces.

A preliminary version of this work has been presented at the International Conference on Medical Image Computing and Computer Assisted Intervention (MICCAI)(Lam et al., 2014a). This paper is a significant extension of the preliminary version with more details about the proposed methodology, and more extensive validations. Moreover, new experiments have been added to demonstrate the stability of the registration algorithm under geometric noises and to illustrate the inverse consistency property of the obtained T-Map.

The rest of the paper is organized as follows. In section 2, we introduce some basic mathematical concepts relevant to this work. In section 3, we describe our proposed surface registration model in details. The numerical implementation details will be presented in section 4. Experimental results will be summarized in section 5. Conclusion and future works will be discussed in section 6.

2. Some basic mathematical background

In this section, we describe some relevant mathematical concepts. For details, we refer the readers to (Gardiner and Lakic, 2000).

A Riemann surface M is an oriented manifold of dimension two together with a metric tensor $\mathbf{g} : M \to M_{2\times 2}(\mathbb{R})$. The *genus* of a Riemann surface is the number of handles on it. For example, a sphere is of genus zero, whereas a standard torus and a vertebral bone are both of genus one (see Figure 1(a) and (b)). This work focuses on Riemann surfaces of genus one. Every genus-one surface M can be sliced open by cutting it along the boundary cuts, called the *homotopic loops*. The open surface $\hat{M}$, called the *fundamental domain*, can be conformally embedded (parameterized) into one piece of domain in $\mathbb{R}^2$, called the *fundamental polygon*. A parameterization $\phi : \hat{M} \to \mathbb{R}^2$ is called *conformal* if the

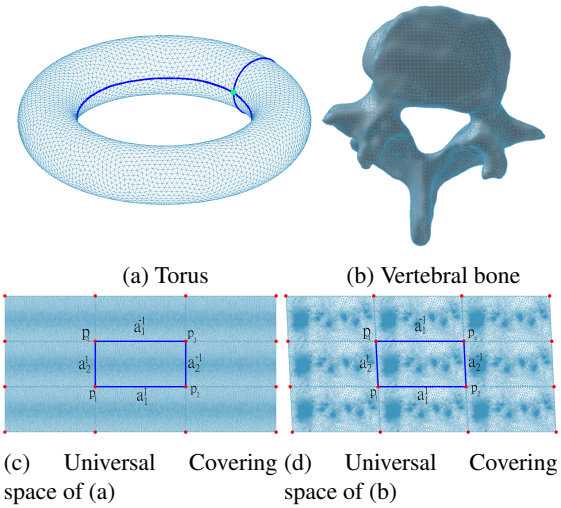

(a) Torus (b) Vertebral bone

(c) Universal Covering space of (a) (d) Universal Covering space of (b)

Figure 1: (a) shows a standard genus-one torus. The torus is cut open along the homotopic loops. (c) shows the fundamental polygon of the standard torus. Figure (b) shows a vertebral bone, which is of genus-one. It is cut open along the homotopic loops. (d) shows the universal convering space.

metric after the transformation of ϕ is preserved up to a (real positive) scaling factor $\lambda : D \to \mathbb{R}^+$, called the *conformal factor*:

$$\mathbf{g} = \lambda \phi^*(dx^2 + dy^2), \tag{1}$$

where ϕ^* is the pull-back map. Note that cutting along each homotopic loops gives rise to two boundary curves of $\hat{M}$, each of which represents the same set of vertices of the original surface M. Thus, each boundary edge of the fundamental polygon is identified with the opposite boundary edge. We can denote the boundary edges of the fundamental domain by $\{a_1, a_2, a_1^{-1}, a_2^{-1}\}$, where a_i and a_i^{-1} are opposite edges ($i = 1, 2$). By glueing infinitely pieces of fundamental domains together along their edges, we obtain the *universal covering space* of M, which is $\mathbb{R}^2$ for a genus-one surface. (See Figure 1(c) and (d))

This work is related to quasi-conformal(QC) maps. A QC map $f : M \to N$ is an orientation-preserving homeomorphism between two surfaces M and N with bounded conformality distortions. The conformality distortion is measured by the *Beltrami differential*. A Beltrami differential is a collection of complex-valued function $\mu_\alpha : U_\alpha \subset M \to \mathbb{C}$ defined on each coordinate chart (U_α, ϕ_α) of M with $\|\mu_\alpha\|_\infty < 1$. It satisfies the

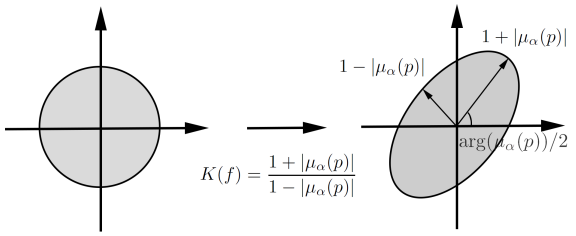

Figure 2: Illustration of how the conformality distortion can be determined by the Beltrami differential.

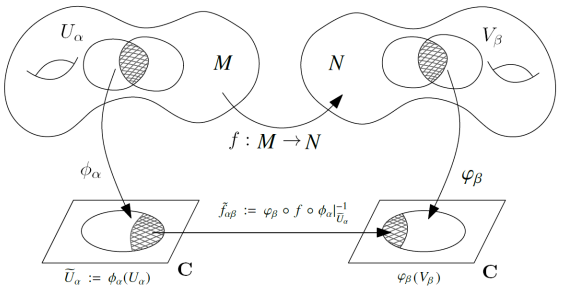

Figure 3: Illustration of surface Quasi-conformal map.

Beltrami's equation:

$$\frac{\partial \widetilde{f}_{\alpha\beta}}{\partial \bar{z}} = \mu_\alpha \frac{\partial \widetilde{f}_{\alpha\beta}}{\partial z}, \tag{2}$$

where $\tilde{f}_{\alpha\beta} := \varphi_\beta \circ f \circ \phi_\alpha|^{-1}_{\widetilde{U}_\alpha}$, $\widetilde{U}_\alpha := \phi_\alpha(U_\alpha)$ and $\varphi_\beta : V_\beta \to \mathbb{R}^2$ is a coordinate chart covering $f(U_\beta) \subset N$. Here, $\frac{\partial}{\partial \bar{z}} := \frac{1}{2}(\frac{\partial}{\partial x} - i\frac{\partial}{\partial y})$ and $\frac{\partial}{\partial z} := \frac{1}{2}(\frac{\partial}{\partial x} + i\frac{\partial}{\partial y})$. (See Figure 3 for an illustration) The Beltrami differential also satisfies the consistency condition on regions covered by two or more coordinate charts. Suppose $p \in M$ is covered by two charts $\phi_\alpha : U_\alpha \to \mathbb{R}^2$ and $\phi_\gamma : U_\gamma \to \mathbb{R}^2$. Then, $\mu_\alpha(p)$ and $\mu_\gamma(p)$ satisfy:

$$\mu_\gamma(p)\frac{\partial \Psi_{\alpha\gamma}}{\partial \bar{z}} = \mu_\alpha(p)\frac{\partial \Psi_{\alpha\gamma}}{\partial z}, \tag{3}$$

where $\Psi_{\alpha\gamma} := \phi_\gamma \circ \phi_\alpha^{-1}$. Intuitively, a quasi-conformal map deforms an infinitesimal circle on M to an infinitesimal ellipse on N. Suppose the Beltrami differential at $p \in M$ is given by $\mu_\alpha(p)$. The distortion from a circle to an ellipse can be measured by the *maximal dilation* K, which can be expressed as:

$$K(f) = \frac{1+|\mu_\alpha(p)|}{1-|\mu_\alpha(p)|}. \tag{4}$$

The maximal stretching and the maximal shrinkage of the deformed ellipse can be measured by $1+|\mu_\alpha(p)|$ and $1-|\mu_\alpha(p)|$ respectively. f is conformal if $|\mu_\alpha(p)| = 0$. In this case, an infinitesimal circle at p is deformed to an infinitesimal circle on N. In other words, the Beltrami differential measures the degree of conformality distortion under f (see Figure 2).

In addition, the Jacobian $J(\widetilde{f}_{\alpha\beta})(p)$ of $\widetilde{f}_{\alpha\beta}$ at p is related to $\mu(p)$ by:

$$J(\widetilde{f}_{\alpha\beta})(p) = |\frac{\partial \widetilde{f}_{\alpha\beta}}{\partial z}|^2(1-|\mu_\alpha(p)|^2) \tag{5}$$

Therefore, $\widetilde{f}_{\alpha\beta}$ is locally injective if $\|\mu_\alpha\|_\infty < 1$ on every coordinate charts.

Ideally, we look for a surface map that is perfectly conformal. However, a perfect conformal map between two genus-one surfaces, which aligns corresponding feature landmarks consistently, may not exist. In this work, our goal is to search for a landmark-matching surface map that minimizes the conformality distortion. Such surface mapping is called the *Teichmüller extremal map* or simply the *Teichmüller map (T-Map)*, which will be explained in details in the next section.

3. Genus-one surface Teichmüller map

In this section, we describe our proposed model to obtain the landmark-constrained genus-one Teichmüller map for surface registration. Let M and N be genus-one surfaces. We label corresponding landmarks $\{r_k \in M\}_{k=1}^m$ and $\{s_k \in N\}_{k=1}^m$ respectively. Our problem can be formulated as finding an optimal surface map $f : M \to N$ that minimizes:

$$E_B(f) = \max_{\alpha \in I} \|\mu_\alpha(f)\|_\infty, \tag{6}$$

subject to: $f(r_k) = s_k$ for $k = 1, 2, ..., m$ *(landmark constraints)*. Here, I is the index set for all coordinate charts covering M.

3.1. Overall framework

We first give an overview of the overall framework to compute the landmark constrained genus-one surface Teichmüller map. It consists of two main steps.

Step 1. To simplify the computation, we first conformally embed M and N into $\mathbb{R}^2$. Thus, all computations can be processed on $\mathbb{R}^2$.

Step 2. Compute the landmark constrained Teichmüller map of $\mathbb{R}^2$ using an iterative scheme, called the *quasi-conformal(QC) iteration*.

As a result, the landmark constrained genus-one surface Teichmüller map can be obtained by the composition map with the parameterizations.

We remark that the computation of T-Map for simple (simply-connected) surfaces have been considered in Lui et al. (2014b). For high-genus surfaces, the computation is much more challenging for the complicated topologies of the surfaces. In this paper, we propose a novel method to compute the landmark constrained T-Map between genus-one surfaces. As far as we know, it is the first work handling this challenging problem. It is also the first work to introduce Teichmüller extremal maps to medical imaging for surface registration problems.

The geometric illustration of the overall framework is shown in Figure 4. We will now describe each step in details.

3.2. Conformal flattening

The embedding of the genus-1 surface is computed using the Ricci flow method introduced by Jin et al. (2008). The basic idea of Ricci flow is to conformally deform the metric $g = (g_{ij}(t))$ according to its induced Gaussian curvature $K(t)$. Mathematically, we have

$$\frac{dg_{ij}(t)}{dt} = -2(K(t) - \bar{K})g_{ij}(t) \tag{7}$$

where we set $\bar{K} = 0$ for genus-one surfaces. Convergence of this process is guaranteed by Hamilton's theorem. $g(\infty)$ is the desired uniformization metric. Let S be a genus-1 surface and p be a base point for S. Two closed loops based at p are introduced to slice the genus-1 surface into the fundamental domain. With the uniformization metric, the fundamental domain can be conformally embedded onto a 2D domain $\Omega \in \mathbb{R}^2$, called the fundamental polygon (See Figure 1(c)). Denote the boundaries and vertices of the polygon as $\{a_1, a_2, a_1^{-1}, a_2^{-1}\}$ and $\{p_i\}_{i=1}^4$ respectively. The boundary pairs $\{a_1, a_1^{-1}\}$,$\{a_2, a_2^{-1}\}$ and vertices $\{p_i\}_{i=1}^4$ correspond to the closed loop and the single based point introduced. Note that a_i and a_i^{-1}, $i = 1, 2$ are related by $\varphi_i(a_i) = a_i^{-1}$, where φ_i are translations in $\mathbb{R}^2$. Therefore, periodic constraints are enforced in the boundaries of the fundamental polygon. With this conformal parameterization, registration can be done on the fundamental domains instead of the complex genus-1 surfaces. For details about the Ricci flow algorithm, we refer the readers to Jin et al. (2008).

3.3. Genus-one surface Teichmüller map

Denote the universal covering maps of M and N by $\pi_M : \mathbb{R}^2 \to M$ and $\pi_N : \mathbb{R}^2 \to N$. Our goal is to look for a quasi-conformal map $f : M \to N$, which minimizes the supreme norm of the Beltrami differential as well as satisfying the landmark constraints.

With the conformal flattenings of genus-one surfaces M and N, the Beltrami differential consists of one complex-valued function $\mu : M \to \mathbb{C}$, which is called the *Beltrami coefficient(BC)*. More precisely, the value of μ at $v \in M$ can be computed as follows. Let U and V be opening neighbourhoods of $v \in M$ and $f(v) \in N$ respectively. Both $\pi_M^{-1}(U)$ and $\pi_N^{-1}(V)$ can be expressed as disjoint unions of connected components in $\mathbb{R}^2$. We take one connected component $\widetilde{U} \subset \pi_M^{-1}(U)$ and one connected component $\widetilde{V} \subset \pi_N^{-1}(V)$. Then, $\mu(p)$ can be computed as:

$$\mu(v) = \left(\frac{\partial \tilde{f}}{\partial \bar{z}}\right) \Big/ \left(\frac{\partial \tilde{f}}{\partial z}\right) \tag{8}$$

where $\tilde{f} := \pi_N|_{\widetilde{V}}^{-1} \circ f \circ \pi_M|_{\widetilde{U}}$.

Now, let Ω_1 and Ω_2 be the fundamental polygons in the universal covering spaces of M and N respectively. Thus, $\pi_M|_{\Omega_1} : \Omega_1 \to M$ and $\pi_N|_{\Omega_2} : \Omega_2 \to N$ are diffeomorphisms. We further assume the four vertices $\mathcal{P} = \{p_i\}_{i=1}^4$ of Ω_1 correspond to the four vertices $\mathcal{Q} = \{q_i\}_{i=1}^4$ of Ω_2. Suppose $\{p \in M\} = \pi_M(\mathcal{P})$ and $\{q \in N\} = \pi_N(\mathcal{Q})$. Then, p and q must correspond with each others, which can be chosen as a pair of corresponding landmark points on M and N respectively.

To compute the genus-one surface Teichmüller map between M and N, we look for injective map $\widetilde{f} : \Omega_1 \to \mathbb{R}^2$ such that $f = \pi_N \circ \widetilde{f} \circ \pi_M|_{\Omega_1}^{-1} : M \to N$ is our desired optimal quasi-conformal surface map solving optimization problem (6).

Note that according to the construction, $\widetilde{\Omega}_2 := \widetilde{f}(\Omega_1)$ must be a fundamental polygon in the universal covering space of N. In other words, we require that homotopic loops on M are mapped to a set of homotopic loops on N under f. One important feature of our registration algorithm is that it is independent of the cutting boundaries (homotopic loops). More specifically, suppose $\{a_M, b_M, a_M^{-1}, b_M^{-1}\}$ and $\{a_N, b_N, a_N^{-1}, b_N^{-1}\}$ are the edges of Ω_1 and Ω_2 respectively. Let $\hat{a}_M = \pi_M(a_M)$, $\hat{b}_M = \pi_M(b_M)$, $\hat{a}_N = \pi_N(a_N)$ and $\hat{b}_N = \pi_N(b_N)$. Then, $\{\hat{a}_M, \hat{b}_M\}$ and $\{\hat{a}_N, \hat{b}_N\}$ are sets of homotopic loops on M and N respectively. Our algorithm does not require that $f(\hat{a}_M) = \hat{a}_N$ and $f(\hat{b}_M) = \hat{b}_N$. In other words, we allow $f(\hat{a}_M)$ and $f(\hat{b}_M)$ to move freely on N, subject to the condition that they form a set of homotopic loops

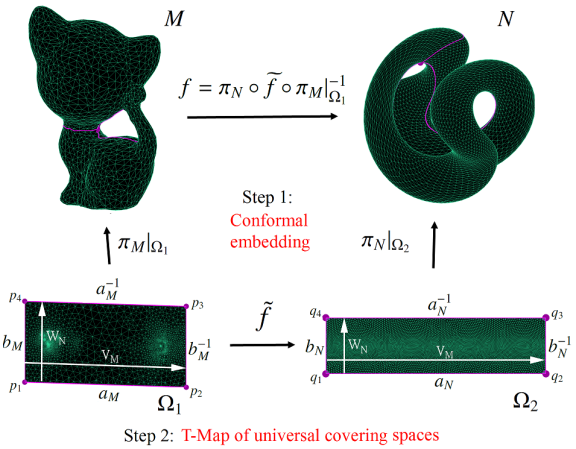

Figure 4: Geometric illustration of the overall framework of our proposed registration algorithm.

on N. To achieve this, $\widetilde{f} : \Omega_1 \to \mathbb{R}^2$ should satisfy the following periodic boundary conditions:

$$\begin{aligned} \widetilde{f}(\mathbf{x} + \mathbf{v}_M) &= \widetilde{f}(\mathbf{x}) + \mathbf{v}_N \text{ for } \mathbf{x} \in a_M; \\ \widetilde{f}(\mathbf{y} + \mathbf{w}_M) &= \widetilde{f}(\mathbf{y}) + \mathbf{w}_N \text{ for } \mathbf{y} \in b_M; \end{aligned} \tag{9}$$

where $\mathbf{v}_M = p_2 - p_1$, $\mathbf{w}_M = p_4 - p_1$, $\mathbf{v}_N = q_2 - q_1$ and $\mathbf{w}_N = q_4 - q_1$. Please refer to Figure 4 for an illustration.

Furthermore, a surface map that minimizes the supreme norm of its Beltrami differential is called an *extremal map*. Therefore, the optimizer for Problem (6) (and also for Problem (11)) is an extremal map that satisfies the prescribed landmark constraints. According to the Teichmüller theory, the extremal map must exist. With the prescribed landmark constraints, the extremal map is also unique. Here, the landmark-matching extremal map can be considered as the optimal quasi-conformal map between M and N with punctures.

Another class of surface maps, called the *Teichmüller maps (T-Maps)*, is closely related to the extremal map. Intuitively, a T-Map is a quasi-conformal map with uniform distribution of conformality distortions. Mathematically, a quasi-conformal map $g : M \to N$ is said to be a *T-Map* associated with an integrable holomorphic function $\varphi : M \to \mathbb{C}$ if its associated Beltrami coefficient is of the form:

$$\mu(g) = k\frac{\bar{\varphi}}{|\varphi|} \tag{10}$$

for some positive constant $0 \le k < 1$ and $\varphi \neq 0$. The Beltrami coefficient of this form is said to be of *Teichmüller type*. According to the frame mapping theorem, a non-conformal landmark-matching extremal map must be a T-Map.

Our surface map optimization problem can now be formulated as finding $\widetilde{f} : \Omega_1 \to \mathbb{R}^2$ that minimizes:

$$E(\widetilde{f}) = \|\mu(\widetilde{f})\|_\infty \tag{11}$$

subject to the following constraints:

1. *Landmark constraint:* $\widetilde{f}(r_k) = s_k$ for $1 \le k \le m$.
2. *Base point consistency:* $\widetilde{f}(p_j) = q_j$ for $1 \le j \le 4$.
3. *Periodic boundary conditions:*
   $\widetilde{f}(\mathbf{x} + \mathbf{v}_M) = \widetilde{f}(\mathbf{x}) + \mathbf{v}_N$ for $\mathbf{x} \in a_M$ and
   $\widetilde{f}(\mathbf{y} + \mathbf{w}_M) = \widetilde{f}(\mathbf{y}) + \mathbf{w}_N$ for $\mathbf{y} \in b_M$.
4. *Teichmüller type constraint:* $\mu(\widetilde{f}) = k\frac{\bar{\varphi}}{|\varphi|}$ where, $0 \le k < 1$ and $\varphi : \Omega_1 \to \mathbb{C}$ is integrable holomorphic.

To solve the above minimization problem, we apply an iterative scheme, called the Quasi-conformal(QC) iterations, to compute the desired Teichmüller extremal map. The convergence of the QC iteration to the T-Map can be found in (Lui et al., 2014a).

The basic idea of the QC iterations is to find a sequence of Beltrami coefficients $\{\nu_n\}_{n=1}^{\infty}$ that approaches to the unique admissible Beltrami coefficient ν^* of Teichmüller type. In each iteration, the iterative algorithm projects the Beltrami differential to the space of all Beltrami differentials of constant modulus, and computes a quasi-conformal map whose Beltrami differential is closest to the projection in the least square sense.

A crucial step in the iterative scheme is to find a quasi-conformal map $\tilde{f}_n$ whose BC is closest to a given ν_n. We will obtain $\tilde{f}_n$ by solving an elliptic PDE. Suppose $\tilde{f}_n = u + iv$ has BC exactly equals to $\nu_n = \rho + i\tau$. From the Beltrami equation (2),

$$\mu(f) = \frac{(u_x - v_y) + i(v_x + u_y)}{(u_x + v_y) + i(v_x - u_y)} \tag{12}$$

Let $\mu(f) = \rho + i\tau$. We have the following linear combinations between u_x, u_y, v_x and v_y:

$$\begin{cases} -v_y &= \alpha_1 u_x + \alpha_2 u_y \\ v_x &= \alpha_2 u_x + \alpha_3 u_y \end{cases} ; \quad \begin{cases} -u_y &= \alpha_1 v_x + \alpha_2 v_y \\ u_x &= \alpha_2 v_x + \alpha_3 v_y \end{cases} \tag{13}$$

where $\alpha_1 = \frac{(\rho-1)^2+r^2}{1-\rho^2-r^2}$; $\alpha_2 = \frac{2r}{1-\rho^2-r^2}$; $\alpha_3 = \frac{1+2\rho+\rho^2+r^2}{1-\rho^2-r^2}$.
By taking divergence on both sides of equations (13), we obtain

$$\nabla \cdot \left(A \begin{pmatrix} u_x \\ u_y \end{pmatrix} \right) = 0; \quad \nabla \cdot \left(A \begin{pmatrix} v_x \\ v_y \end{pmatrix} \right) = 0, \tag{14}$$

where $A = \begin{pmatrix} \alpha_1 & \alpha_2 \\ \alpha_2 & \alpha_3 \end{pmatrix}$. In practice, the prescribed BC ν_n may not be associated to a surface quasi-conformal map subject to the constraints (1), (2) and (3) in Problem (11). Therefore, we solve equation (14) for $\tilde{f}_n$ subject to the constraints (1), (2) and (3) in Problem (11) in the least square sense. We denote the obtained quasi-conformal map by $\widetilde{f_n} = \mathbf{QC}(\nu_n)$.

Now, the iterative scheme to compute the Teichmüller map can be described as follows. We start with setting $\nu_0 = 0$ and search for an initial map $\widetilde{f_0} := \mathbf{QC}(\nu_0 = 0)$ satisfying constraints (1), (2) and (3). Note that with the enforced landmark constraints, the Beltrami coefficient associated to $\widetilde{f_0}$ may not be equal to $\nu_0 = 0$. In other words, ν_0 may not be *admissible*. $\mathbf{QC}(\nu_n)$ simply gives us a quasi-conformal map $\widetilde{f_0}$ whose BC resemble to ν_0 as much as possible. Let $\mu_0 = \mu(\widetilde{f_0})$ be the actual BC of $\widetilde{f_0}$.

The BC of our desired T-Map must be of the Teichmüller type. To obtain a BC of the Teichmüller type, we perform a projection $\mathcal{P}$ and smoothing $\mathcal{L}$ on μ_0. The projection operator $\mathcal{P}$ projects μ_0 to a BC with constant norm. It is defined as follows.

$$\mathcal{P}(\mu) = \begin{cases} \left(\int_{\Omega_1} |\mu| d\Omega_1 \Big/ \int_{\Omega_1} d\Omega_1 \right) \frac{\mu}{|\mu|} & \text{if } \mu \neq 0 \\ 0 & \text{if } \mu = 0 \end{cases}$$

The smoothing operator $\mathcal{L}$ is chosen to be the standard Laplace smoothing. It aims to obtain a smooth BC associated to a smooth quasi-conformal map. Thus, we obtain a new BC: $\nu_1 := \mathcal{L} \circ \mathcal{P}(\mu_0)$. An updated quasi-conformal map $\widetilde{f_1}$ can then be obtained by $\widetilde{f_1} := \mathbf{QC}(\nu_1)$. Again, ν_1 may not be admissible. We compute the actual BC of $\widetilde{f_1}$ and denote it by $\mu_1 := \mu(\widetilde{f_1})$.

We continue the procedure until the iteration converges. More specifically, given $\widetilde{f_n}$ and $\mu_n := \mu(\widetilde{f_n})$ at the n iteration, we obtain a new BC given by $\nu_{n+1} = \mathcal{L} \circ \mathcal{P}(\mu_n)$. An updated quasi-conformal map can be obtained by: $\widetilde{f_{n+1}} = \mathbf{QC}(\nu_{n+1})$. We then compute its actual BC and denote it by $\mu_{n+1} = \mu(\widetilde{f_{n+1}})$.

As a result, we obtain a sequence of Beltrami coefficients $\nu_n : \Omega_1 \to \mathbb{C}$, which converges to an optimal admissible BC ν^* of Teichmüller type. The optimal BC ν^* is associated to our desired Teichmüller extremal map, which can be computed by: $\widetilde{f} = \mathbf{QC}(\nu^*)$. In practice, we stop the iteration when $\|\nu_{n+1} - \nu_n\| < \epsilon$.

The whole process of computing the genus-one surface Teichmüller map can be summarized in Algorithm 1. For the convergence of Algorithm 1, we refer the readers to Lui et al. (2014a).

Algorithm 1: QC-iteration

Input: Ω_1 and Ω_2; landmark constraints $\{r_k\}_{k=1}^m$ and $\{q_k\}_{k=1}^m$.

Output: Optimal Beltrami coefficient ν and the Teichmüller extremal map f

Initial: $\nu_0 = 0$;

repeat

  Update $f = (u, v)$ by solving (14) with ν_{n+1} and constraints (1),(2) and (3);

  Compute $\mu_{n+1} := \mathcal{L}(\mathcal{P}(\nu_n))$, where $\mathcal{L}$ is the laplace smoothing operator and

$$\mathcal{P}(\mu) = \int_{\Omega_1} |\mu| d\Omega_1 \Big/ \int_{\Omega_1} d\Omega_1;$$

  Update $f = (u, v)$ by solving (14) with μ_{n+1} and constraints (1),(2) and (3);

  Set $\nu_{n+1} := \mu(f)$, where $\mu(f)$ is the Beltrami coefficients of f

until $\|\nu_{n+1} - \nu_n\|_\infty \leq \epsilon$;

4. Numerical implementation

In this section, numerical implementation of our proposed algorithms is discussed in details. Suppose $K_M = \left(\{v_i^M\}_i, \{T_j^M\}_j\right)$ and $K_N = \left(\{v_i^N\}_i, \{T_j^N\}_j\right)$ are the meshes of two genus-1 surfaces M and N respectively, where v_i^* and T_i^* are respectively the vertices and triangular faces of the meshes.

4.1. Beltrami coefficients (BC)

Note that according to our setting, the T-Map is computed in 2D. Thus the BC is computed in 2D. In discrete 2D case, a deformation $f = (f_1, f_2)$ of a triangular face $T = (v_1, v_2, v_3)$ can be represented by a linear transformation $A_T = \{a_{ij}\}$:

$$\begin{pmatrix} f_1(v_k) \\ f_2(v_k) \end{pmatrix} = A_T \begin{pmatrix} v_k(x) \\ v_k(y) \end{pmatrix} \quad k = 1, 2, 3. \tag{15}$$

where $v_k(x)$ and $v_k(y)$ are the x- and y-coordinates of the vertex v_k respectively. Therefore, the partial derivatives of f can be seen as:

$$\frac{\partial f_k}{\partial x} = a_{k1}; \quad \frac{\partial f_k}{\partial y} = a_{k2}, \quad k = 1, 2 \tag{16}$$

By equation (12), we define the discrete Beltrami coefficient BC at triangular face T by:

$$\mu(T) = \frac{(a_{11} - a_{22}) + \sqrt{-1}\,(a_{21} + a_{12})}{(a_{11} + a_{22}) + \sqrt{-1}\,(a_{21} - a_{12})} \tag{17}$$

We also approximate the BC $\mu(v_i)$ at vertex v_i by

$$\mu(v_i) = \frac{1}{|N_i|} \sum_{T \in N_i} \mu(T) \tag{18}$$

where N_i is the collection of neighborhood faces attached to v_i. In other words, $\mu(v_i)$ is the average of the Beltrami coefficients $\mu(T)$ over a 1-ring neighbourhood triangles.

4.2. Laplacae smoothing operator $\mathcal{L}$

In step 4 of **Algorithm 1**, the laplace smoothing operator $\mathcal{L}$ is applied on both the norm and the argument of ν_n independently, where $\mathcal{L}$ is defined as:

$$\mathcal{L}(\nu_n)(T) = L(T)e^{i\Theta(T)} \tag{19}$$

where

$$L(T) = \sum_{T_i \in N(T)} \frac{|\nu_n(T_i)|}{|N(T)|}, \quad \text{and} \quad \Theta(T) = \sum_{T_i \in N(T)} \frac{\arg(\nu_n)}{|N(T)|} \tag{20}$$

When ν_n is not a constant, the laplace smoothing on $|\nu_n|$ diffuses the norm of ν_n and hence decreases the L^∞-nom of ν_n. The smoothing on the argument of ν_n is also crucial to guarantee the argument of ν_n is harmonic, which in turns guarantee the argument of the optimal Beltrami coefficients μ^* is equal to the argument of a holomorphic function φ (See equation 10).

4.3. Projection operator $\mathcal{P}$

The discrete projection operator $\mathcal{P}$ in step 4 of the algorithm is defined as

$$\mathcal{P}(\nu_n)(T) := \left(\frac{\sum_{T \in K(T)} |\nu_n(T)|}{|K(T)|} \right) \frac{\nu_n(T)}{|\nu_n(T)|} \tag{21}$$

where $K(T)$ is the set of all triangular faces of the mesh K. Notice that $\mathcal{P}(\nu_n) < \|\nu_n\|_\infty$ until ν_n has a constant norm.

4.4. Discretization of $\mathcal{QC}$

Without considering any constraints in the optimization problem (11), the elliptic PDEs (14) can be discretized into sparse positive definition linear systems $\mathcal{E}$ by using the one-ring neighborhood of the mesh. For the base points or landmark points v_i , we set $\mathcal{E}(v_i, v_i) = 1, \mathcal{E}(v_i, v_j) = 0$ if $v_j \neq v_i$. The linear system then becomes $\mathcal{E}(f(v_i)) = b$, where b is a zero vector except at v_i with $b(v_i) = f(v_i)$.

Since the surfaces we are considering are genus-1, the deck transformations, i.e. the periodic boundary conditions defined on the boundaries of the fundamental domain, is linear and can be represented by a translation κ. Then for any vertices v_i on the boundary of the fundamental domain, let

$$\mathcal{E}(f(v_i)) = \sum_{j \in N(v_i)} e_{ij}(f(v_j) - f(v_i)) + \sum_{j \in \widetilde{N}(v_i)} e_{ij}(f(v_j) - f(v_i)) \tag{22}$$

where $N(v_i)$ and $\widetilde{N}(v_i)$ are the sets of vertex indices of the one-ring neighbors of vertex v_i which are inside and outside the fundamental domain respectively. Denote v'_j to be the inside copy of the vertex v_j, where v_j is outside the fundamental domain, we then have

$$\begin{aligned} \mathcal{E}(f(v_i)) &= \sum_{j \in N(v_i)} e_{ij}(f(v_j) - f(v_i)) + \\ &\quad \sum_{j' \in \widetilde{N}(v'_i)} (f(v'_j) - f(v'_i)) \\ &= \sum_{j \in N(v_i)} e_{ij}(f(v_j) - f(v_i)) + \\ &\quad \sum_{j \in \widetilde{N}(v_i)} (\kappa(f(v_j)) - \kappa(f(v_i))) \end{aligned}$$

In matrix form, the modified elliptic PDEs are:

$$\mathcal{E}(f(v_i)) + Q(v_i) = b \tag{23}$$

where Q is the linear operator that transforms outside neighborhood vertices v_j of v_i to its inside copy v'_j and is zero elsewhere. By solving the equation, the associated quasi-conformal map f of $\mu(f)$ satisfying the periodic boundary conditions can be obtained.

5. Experimental results

To evaluate our proposed algorithm, we apply it to register genus-one vertebrae bone surfaces using Teichmüller extremal map. In this section, we report the experimental results.

5.1. Vertebrae bone registration

We test our algorithm to register 10 corresponding vertebrae bones from 10 subjects. Each vertebrae bone surface is labelled with prescribed feature points and curves as landmarks. Figure 5 shows two vertebrae bones with corresponding feature landmarks labeled on each of them. There are two landmark curves labelled on the top and bottom side of the cortical rim and ten feature points marked on other parts of each vertebral bone.

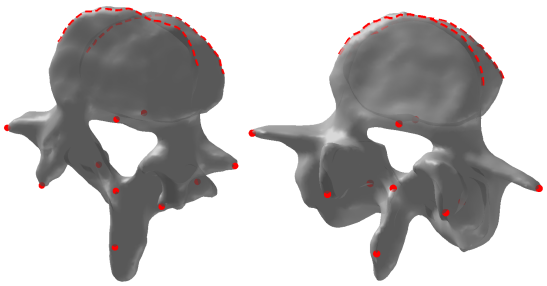

(a) Vertebrae S_1 (b) vertebrae S_2

Figure 5: The figure shows two vertebrae bones S_1 and S_2 with corresponding feature landmarks labeled on each of them.

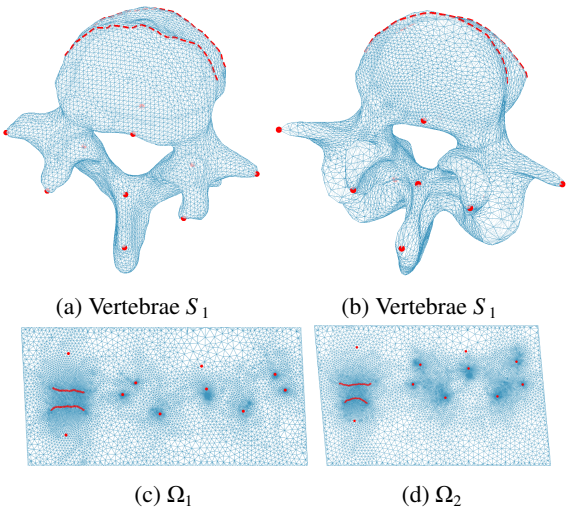

(a) Vertebrae S_1 (b) Vertebrae S_1 (c) Ω_1 (d) Ω_2

Figure 6: (a) and (b) shows the triangulation meshes of the two vertebrae bones in Figure 4. (c) and (d) shows their fundamental domains obtained using the Ricci flow method.

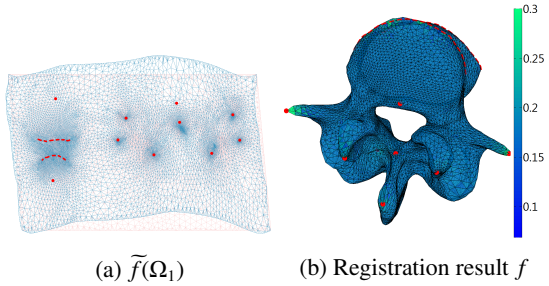

(a) $\widetilde{f}(\Omega_1)$ (b) Registration result f

Figure 7: (a) shows the obtained Teichmüller map on the universal covering space of S_2. (b) shows the obtained surface registration result obtained from the composition map.

To register between a pair of vertebrae bones S_1 and S_2, we first embed the surfaces into $\mathbb{R}^2$ by the Ricci flow method (Jin et al., 2008). The two surfaces are conformally mapped to their fundamental polygons. Denote the fundamental polygons of S_1 and S_2 by Ω_1 and Ω_2 respectively. Figure 6(a) and (b) show a pair of vertebrae bone surfaces. Figure 6(c) and (d) show their corresponding fundamental polygons in $\mathbb{R}^2$. Using QC iteration as described in Section 3, the Teichmüller extremal map $\widetilde{f} : \Omega_1 \to \mathbb{R}^2$, which satisfies the landmark constraints, is obtained. Since no hard constraint is enforced for $\widetilde{f}$ on the boundary edges of Ω_1, the boundaries of the target domain $\widetilde{f}(\Omega_1)$ can move freely on the universal covering space, which satisfy the periodic conditions. Figure 7(a) shows the obtained Teichmüller extremal map on the universal covering space of S_2. It shows how the mesh of Ω_1 is transformed under $\widetilde{f}$. Note that $\widetilde{f}(\Omega_1)$ is different from the original fundamental polygon Ω_2 of S_2. Yet, the boundary edges of $\widetilde{f}(\Omega_1)$ satisfies the periodic boundary conditions, so that $\widetilde{f}(\Omega_1)$ is still a fundamental polygon of S_2. This is crucial to ensure the composition map with the conformal parameterization is a surface map from S_1 and S_2, with the cutting boundaries consistently glued together.

Once the Teichmüller extremal map is computed, we can obtain the registration between the vertebrae S_1 and S_2 by a composition of functions $f := \phi_2^{-1} \circ f \circ \phi_1 = T : S_1 \to S_2$. The resultant registration is shown in Figure 7(b). The mesh is obtained by deforming the source vertebral bone (Figure 6(a)) to the target surface (Figure 6(b)). Landmark curves and feature points are exactly matched after the registration process. Figure 7(b) also shows $|\mu(f)|$ of the Teichmüller extremal mapping, which is represented by the color map on the vertebral bone surface. An even color distribution on the surface and a small standard deviation of the BC norm of 0.001823 indicate that the resultant mapping is actually of Teichmüller type.

Figure 9(a) shows the plot of energy $E(\widetilde{f}_n)$ versus iterations. The energy decreases as iteration increases. Our registration model iteratively compute the optimal quasi-conformal map that minimizes the conformality distortion.

By the properties of Teichmüller map, the registration obtained is guaranteed to be folding-free. To demonstrate this property quantitatively, we compute the Jacobian of the mapping at each faces (See Figure 9(b)). Note that the smallest values of the Jacobian over all faces is 0.3, which is non-zero. Since the Jacobian is non-zero everywhere, we can conclude that the obtained registration is folding-free.

An important feature of our registration model is that it computes surface mappings, which match corresponding feature landmarks consistently. We evaluate this property as follows. We first compute Teichmüller

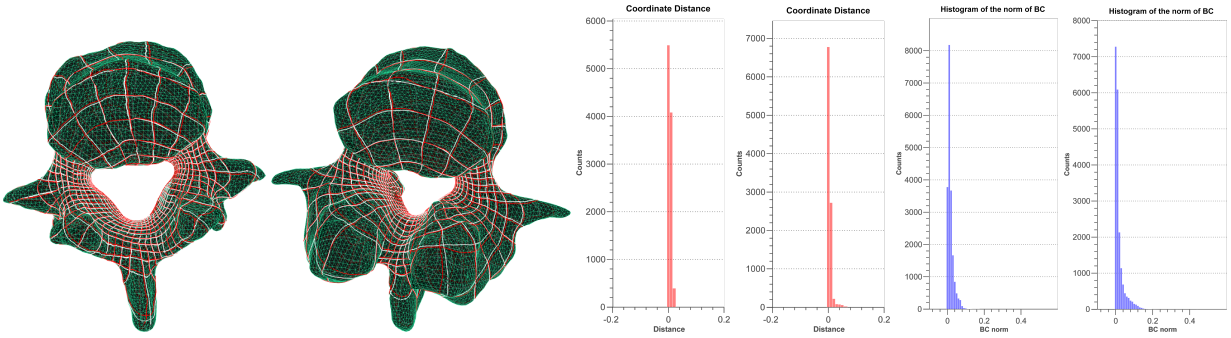

(a) Vertebrae S_A (b) Vertebrae S_B (c) Coord. Dist. of S_A (d) Coord. Dist. of S_B (e) $\mu(g \circ f)$ of S_A (f) $\mu(g \circ f)$ of S_B

Figure 8: Illustration of the inverse consistency property of the proposed algorithm. The surface registrations $f : S_1 \to S_2$ and $g : S_2 \to S_1$ are both computed. (a) shows how an initial grid (in white color) is deformed by $g \circ f$ to another grid (in red color). The two grids almost overlap with each others (b) shows another example for a different pair of vertebrae bones. (c) and (d) show the histogram of coordinate distances for example (a) and (b) respectively. (e) and (f) show the histograms of $\mu(g \circ f)$ for example (a) and (b) respectively.

extremal mappings between a set of vertebrae bones. We then construct a new surface by computing the average coordinates for each vertices. Figure 10 shows the new surface $S^{average}$. If landmarks are consistently aligned under the Teichmüller extremal maps, the features should be well-preserved on $S^{average}$. As shown in the figure, the feature points and curves on $S^{average}$ are well-preserved. This illustrates that landmarks are consistently matched under the proposed registration algorithm.

We have test the algorithm on 5 pairs of vertebrae bone surfaces. Table 1 shows the statistics of the results. The maximum landmark mismatching error $e_{\max}$, the mean landmark mismatching error e_{mean}, the mean of BC, the standard deviation of the BC and the computation time are reported. Our algorithm takes less than 20 second to compute the surface registration. The mean of BC shows the minimal conformality distortion of the surface registration, given the prescribed landmark constraints. The standard deviation of the BC distribution is small, meaning that the conformality distortion is uniform over every vertices. It demonstrates the obtained surface registrations are indeed Teichmüller extremal maps.

5.2. Inverse consistency

Given the corresponding landmark constraints, a Teichmüller extremal map $f : S_1 \to S_2$ is unique. Let μ_f be the Beltrami coefficient of f. The Beltrami coefficient of f^{-1} is given by:

$$\mu_{f^{-1}} \circ f = -\left(\frac{f_z}{|f_z|}\right)^2 \mu_f \tag{24}$$

Hence, $|\mu_{f^{-1}} \circ f| = |\mu_f|$ is a constant. In fact, f^{-1} is also a T-Map with the given landmark constraints. Since a T-Map is unique, f^{-1} can be obtained by computing a T-Map $g : S_2 \to S_1$ from S_2 to S_1 with given landmark constraints. $g \circ f$ is then an identity map of S_1. In other words, the forward and backward registrations are inversely consistent. Therefore, our registration algorithm is independent on the choice of the source and target surfaces. We have designed experiments to test the inverse consistency property. Given a pair of vertebrae bone surfaces S_1 and S_2, we first compute the T-Map $f : S_1 \to S_2$ by choosing S_1 and S_2 as the source and target surfaces respectively. We then choose S_2 as the source surface and S_1 as the target surface to obtain another T-Map $g : S_2 \to S_1$. $g \circ f : S_1 \to S_1$ should be close to (ideally, equal to) an identity map. Figure 8(a) shows how an initial grid (in white color) is deformed by $g \circ f$ to another grid (in red color). Note that the two grids almost overlap with each others, illustrating that $g \circ f$ is close to identity. Figure 8(b) shows another example for a different pair of vertebrae bones, which again demonstrates the inverse consistency property of our registration algorithm. We have also computed the histograms of $\|g \circ f(p) - p\|$ for the two experiments (See Figure 8(c) and (d)). Note that in all three experiments, $\|g \circ f(v) - v\|$ accumulates at 0. It means that $g \circ f(v) = v$ for most vertices v of S_1. As the mapping $g \circ f$ is close to identity, the corresponding Beltrami coefficients $\mu(g \circ f)$ is also close to 0. The histogram of the BC norm for the two examples are reported in Figure 8(e) and (f) respectively, which validate this observation.

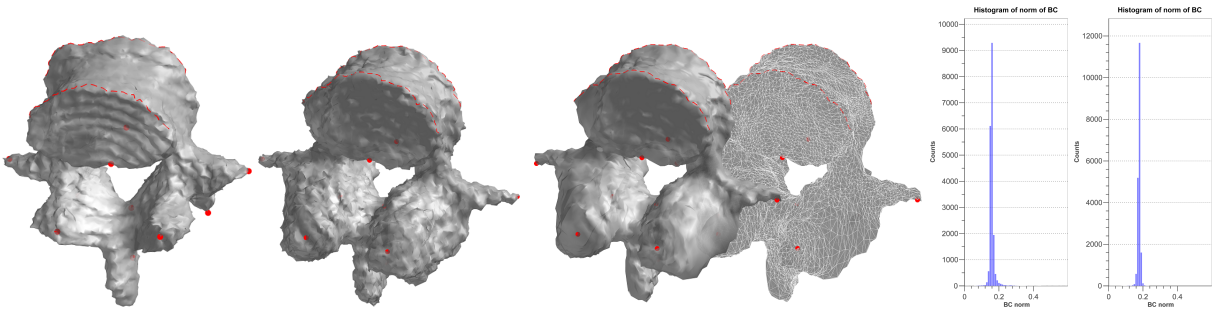

(a) Noisy vertebrae S_1 (b) Noisy vertebrae S_2 (c) Registration result (d) μ without noise (e) μ with noise

Figure 11: Stability under geometric noises. (a) and (b) show a pair of vertebrae bones, which are both corrupted by geometric noises. The surface registration between them using our proposed algorithm is shown in (c). Both the surface and its triangulation mesh are shown. (d) shows the the histogram of the BC norm of the surface T-Map between the original surfaces without the corruption of geometric noises. (e) shows the BC norm of the surface T-Map between the noisy vertebrae bones.

5.3. Stability under geometric noises

Our proposed registration model is also stable under geometric noises. Figure 11(a) and (b) show a pair of vertebrae bones, which are both corrupted by geometric noises. A landmark-matching Teichmüller extremal map can be obtained, despite of the presence of geometric noises. The registered result is shown in Figure 11(c). The histogram of the BC norm is shown in Figure 11(e). The BC norm accumulates at 0.21, meaning that the obtained surface map is indeed a T-Map. We have also computed the surface T-Map between the original surfaces without the corruption of geometric noises. The histogram of the BC norm is shown in Figure 11(d). Note that the histogram in (d) closely resembles to that in (e). This illustrates that our proposed algorithm to compute surface T-Map is stable under geometric noises.

5.4. Stability under landmark selection errors

The selection of feature landmarks can be prone to errors. Our registration algorithm is stable under landmark selection errors. Figure 12(a) and (b) show a pair of vertebrae bones with corresponding landmarks (in blue color) labeled on each of them. We manually distort the landmark positions to get a new set of corresponding landmarks (in red color). We compute two surface T-Maps with respect to the two different sets of corresponding landmarks. Denote the two surface T-Maps by $f_1 : S_1 \to S_2$ and $f_2 : S_1 \to S_2$. The histogram of the coordinate distance $|f_1(v) - f_2(v)|$ between f_1 and f_2 over every vertices v of S_1 is shown in Figure 13(a). Note that the coordinate distance accumulates at a very small value, meaning that our proposed registration model is stable under landmark selection errors. The hisograms of the BC norm of the registrations for original and distorted landmark constraints are also reported in Figure 13(b) and (c) respectively. Note that the histogram in (b) has a similar distribution to the histogram in (c).

5.5. Invariant under cutting boundaries

To validate the invariance of our proposed algorithm under the choice of cutting boundaries, we manually labeled three arbitrary simple closed loops (blue, red and green loops in Figure 14)(a) with the same base point and run the proposed algorithm. Let f_b, f_r and f_g be the surface T-Maps obtained with the blue, red and green cutting boundaries respectively. Figure 14(b),(c) and (d) show the histograms of the optimal Teichmüller type BCs $|\mu(f_g)|$, $|\mu(f_r)|$ and $|\mu(f_b)|$ of f_g, f_r and f_b respectively. Experimental results show that all three registration results are consistent. Also, it is observed that $\||\mu(f_b)|-|\mu(f_r)|\|_\infty = 0.0021$, $\||\mu(f_r)|-|\mu(f_g)|\|_\infty = 0.0044$ and $\||\mu(f_b)| - |\mu(f_g)|\|_\infty = 0.0038$, which are all very small. This indicates that our proposed algorithm is indeed invariant to the choice of cutting boundaries.

5.6. Comparison with other methods

We have also compared our implementation with rigid ICP and non-rigid ICP. The result is summarized in Table 1. For the ease of comparison, we first normalize every vertebral bone to fit into a unit cube. In terms of the mean and maximum landmark matching errors (e_{mean}, e_{max}), our proposed method outperforms the two point-based registration methods. The Hausdorff distance d_H between the registration result and the target also shows that our proposed method has a better

	Rigid ICP			NonRigid ICP			Proposed		
	$e_{\max}$	e_{mean}	$\|\mu\|_\infty$	$e_{\max}$	e_{mean}	$\|\mu\|_\infty$	$e_{\max}$	e_{mean}	$\|\mu\|_\infty$
	SD(μ)	d_H	Time	SD(μ)	d_H	Time	SD(μ)	d_H	Time
f_1	0.1467	0.0389	$1.08e^{-13}$	0.0798	0.0402	0.9841	0	0	0.4193
	$5.33e^{-15}$	12.44	4.46s	0.1710	4.55	223.07s	0.0147	0.82	10.91s
f_2	0.1404	0.0425	$1.44e^{-12}$	0.1275	0.0546	0.9887	0	0	0.2055
	$2.61e^{-14}$	13.32	3.34s	0.1591	3.7719	191.37s	0.0018	1.81	14.46s
f_3	0.2460	0.0739	$1.53e^{-11}$	0.2649	0.0581	0.9632	0	0	0.3312
	$1.17e^{-13}$	13.3224	2.27s	0.1224	4.4804	205.12s	0.0227	4.41	13.62s
f_4	0.1005	0.0819	$6.75e^{-12}$	0.0981	0.0526	0.9679	0	0	0.2235
	$7.06e^{-14}$	11.2640	1.12s	0.1188	5.9625	200.06s	0.0084	2.9464	17.09s
f_5	0.1260	0.576	$6.10e^{-13}$	0.1317	0.0611	0.9648	0	0	0.3480
	$1.66e^{-14}$	16.6272	2.33s	0.1727	5.7175	284.22s	0.0104	3.2470	19.94s

Table 1: Summary of the registration results using different registration methods

overlay percentage to the target object. With the sacrifice of the registration accuracy, almost no conformality distortion is introduced by the rigid ICP, while the non-rigid ICP produces a large distortion of 0.9887. In terms of the landmark matching criterion, our proposed algorthim provides an exact landmark matching result for the vertebrae bone registration, while both ICP and non-rigid ICP induce mismatching error of the feature correspondences.

6. Conclusion

The paper presents a novel algorithm to compute landmark constrained genus-one surface Teichmüller map (T-Map). The proposed algorithm can be applied to landmark-based surface registration for genus-one surfaces. The basic idea of the algorithm is to embed the genus-one surface into its universal covering space in $\mathbb{R}^2$ and compute the T-Map between the fundamental domains using an iterative scheme called the QC iteration. The obtained landmark constrained T-Map is the unique mapping between genus-1 surfaces that minimizes the maximal conformality distortion while matching the prescribed feature landmarks. Existence and uniqueness of the landmark constrained T-Map are theoretically guaranteed. We have tested the proposed algorithm to register genus-one vertebral bone surfaces. Experimental results demonstrate the effectiveness of our proposed algorithm to obtain accurate surface registrations of the vertebral bones. In the future, we will apply the proposed algorithm to register a large dataset of vertebrae bones for disease analysis. We will also extend the proposed algorithm to compute landmark constrained surface T-Map for surfaces of genus greater than 1.

Acknowledgements

This research is supported by the HKRGC GRF (CUHK Project ID: 404612). The author would like to thank Dr. Defeng Wang and Dr. Lin Shi for providing the vertebrae bone data for the testing of the proposed registration algorithm.

References

Bookstein, F.L., 1989. Principal warps - thin-plate splines and the decomposition of deformations. Ieee Transactions on Pattern Analysis and Machine Intelligence 11, 567–585.

Chung, M., Dalton, K., Davidson, R., 2008. Tensor-based cortical surface morphometry via weighted spherical harmonic representation. IEEE Transaction on Medical Imaging 27, 1143–1151.

Chung, M., Worsley, K., Paus, T., Collins, D., Giedd, J., Rapoport, J., Evans, A, C., 2001. A unified statistical approach to deformation-based morphometry. NeuroImage 14, 595–606.

Chung, M., Worsley, K., Robbins, S., Paus, T., Taylor, J., Giedd, J., Rapoport, J., Evans, A, C., 2003. Deformation-based surface morphometry applied to gray matter deformation. NeuroImage 18, 198–213.

Drury, H., Van Essen, D., Anderson, C., Lee, C., Coogan, T., Lewis, J., 1996. Computerized mappings of the cerebral cortex: A multiresolution flattening method and a surface-based coordinate system. J Cognitive Neurosciences 8, 1–28.

Fischl, B., Sereno, M., Dale, A., 1999a. Cortical surface-based analysis ii: Inflation, flattening, and a surface-based coordinate system. NeuroImage 9, 195–207.

Fischl, B., Sereno, M.I., Tootell, R.B.H., Dale, A.M., 1999b. High-resolution intersubject averaging and a coordinate system for the cortical surface. Human Brain Mapping 8, 272–284.

Gardiner, F.P., Lakic, N., 2000. Quasiconformal Teichmüller theory. Mathematical surveys and monographs,, American Mathematical Society.

Glaunès, J., Vaillant, M., Miller, M.I., 2004. Landmark matching via large deformation diffeomorphisms on the sphere. Journal of Mathematical Imaging and Vision 20, 179–200.

Gu, X., Wang, Y., Chan, T., Thompson, P., S.T.:, Y., 2004. Genus zero surface conformal mapping and its application to brain surface mapping. IEEE Transaction on Medical Imaging 23, 949–958.

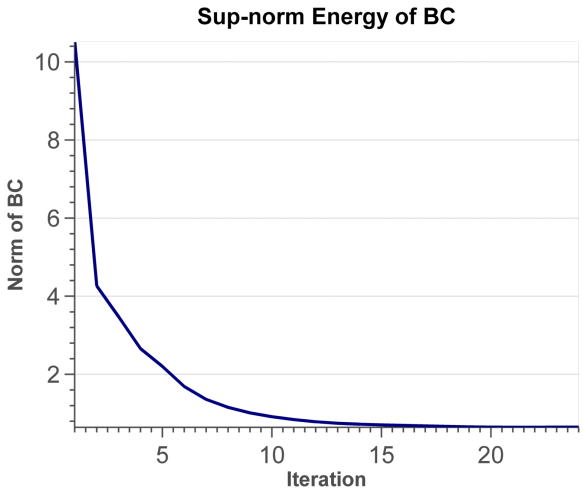

(a) $\|\mu\|_\infty$ versus iterations

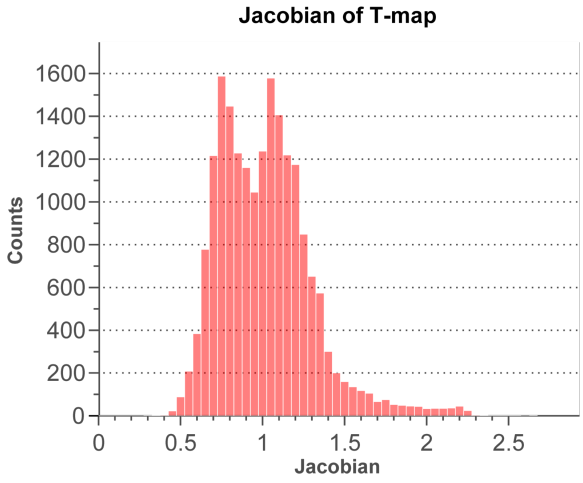

(b) Jacobian of T-map

Figure 9: (a) shows the plot of the energy $E(\widetilde{f})$ versus iterations. (b) shows the histogram of the Jacobian over every triangular faces.

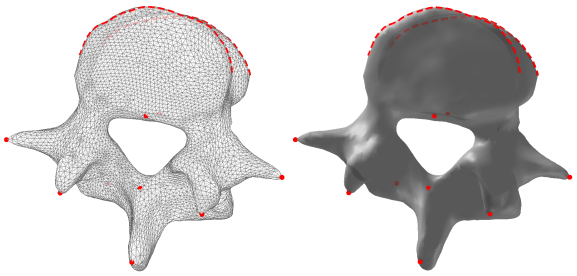

Figure 10: The averaged surface $S^{average}$. The triangular mesh of the surface is shown on the left.

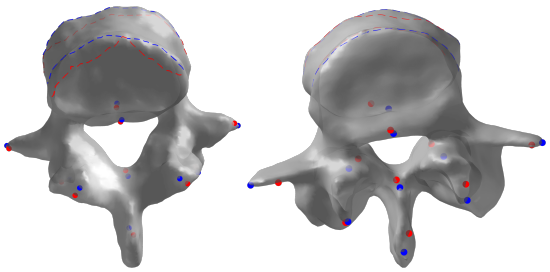

(a) Vertebrae S_1 (b) Vertebrae S_2

Figure 12: Stability under the landmark selection errors. (a) and (b) shows a pair of vertebrae bones with corresponding landmarks (in blue color) labeled on each of them. We manually distort the landmark positions to get a new set of corresponding landmarks (in red color).

Haker, S., Angenent, S., Tannenbaum, A., Kikinis, R., Sapiro, G., 2000. Conformal surface parameterization for texture mapping. Ieee Transactions on Visualization and Computer Graphics 6, 181–189.

Hurdal, M.K., Stephenson, K., 2009. Discrete conformal methods for cortical brain flattening. Neuroimage 45, S86–S98.

Jin, M., Kim, J.H., Luo, F., Gu, X.F., 2008. Discrete surface ricci flow. Ieee Transactions on Visualization and Computer Graphics 14, 1030–1043.

Johnson, H., Christensen, G., 2002. Consistent landmark and intensity-based image registration. IEEE Transactions on Medical Imaging 21, 450–461.

Joshi, S.C., Miller, M.I., 2000. Landmark matching via large deformation diffeomorphisms. Ieee Transactions on Image Processing 9, 1357–1370.

Lam, K., Gu, X., Lui, L., 2014a. Genus-one surface registration via teichmuller extremal mapping. Medical Image Computing and Computer-Assisted Intervention-MICCAI 2014 8675, 25–32.

Lam, K., Lui, L., 2014. Landmark and intensity based registration with large deformations via quasi-conformal maps. SIAM Journal on Imaging Sciences in press.

Lam, K., Wen, C., Lui, L., 2014b. Conformal-based surface morphing and multi-scale representation. Axioms (SI: Discrete Differential Geometry and its Applications to Imaging and Graphics) 2, 222–243.

Lord, N.A., Ho, J., Vemuri, B.C., Eisenschenk, S., 2007. Simultaneous registration and parcellation of bilateral hippocampal surface pairs for local asymmetry quantification. Ieee Transactions on Medical Imaging 26, 471–478.

Lui, L., Wen, C., Gu, X., 2013. A conformal approach for surface inpainting. Journal of Inverse Problems and Imaging 7, 863–884.

Lui, L.M., Gu, X., Yau, S.T., 2014a. Convergence analysis of an iterative algorithm for teichmuller maps via harmonic energy optimization. Mathematics of Computation , in press.

Lui, L.M., Lam, K.C., Yau, S.T., Gu, X.F., 2014b. Teichmuller mapping (t-map) and its applications to landmark matching registration. Siam Journal on Imaging Sciences 7, 391–426.

Lui, L.M., Thiruvenkadam, S., Wang, Y.L., Thompson, P.M., Chan, T.F., 2010a. Optimized conformal surface registration with shape-based landmark matching. Siam Journal on Imaging Sciences 3, 52–78.

Lui, L.M., Wang, Y.L., Chan, T.F., Thompson, P., 2007. Landmark constrained genus zero surface conformal mapping and its application to brain mapping research. Applied Numerical Mathematics 57, 847–858.

Lui, L.M., Wen, C.F., 2014. Geometric registration of high-genus surfaces. Siam Journal on Imaging Sciences 7, 337–365.

Lui, L.M., Wong, T.W., Thompson, P., Chan, T., Gu, X.F., Yau, S.T., 2010b. Shape-based diffeomorphic registration on hippocampal

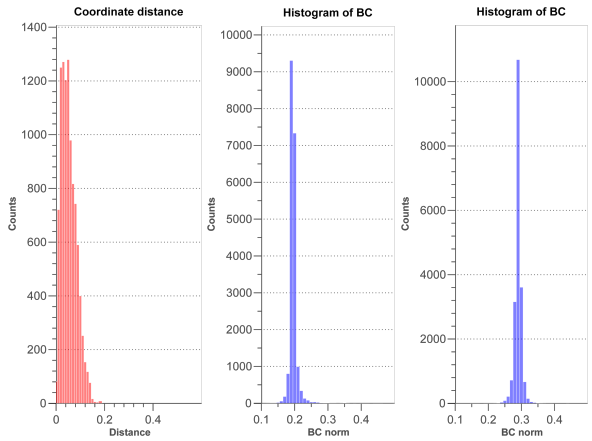

(a) Coordinate Distance (b) Original μ (c) μ with landmark errors

Figure 13: Two surface T-Maps with respect to the two different sets of corresponding landmarks in Figure 11 are computed. (a) shows the historgram of the coordinate distance of the two surface maps.The histograms of the BC norm of the registrations with respect to the original and distorted landmark constraints are shown in (b) and (c) respectively.

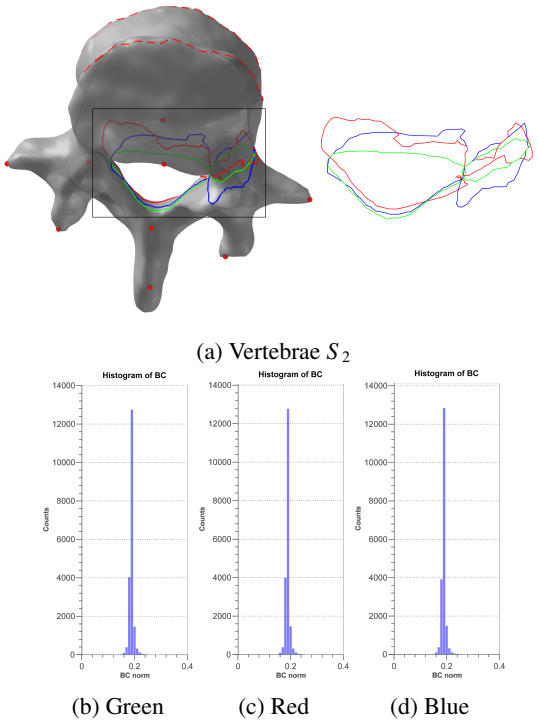

(a) Vertebrae S_2

(b) Green (c) Red (d) Blue

Figure 14: Invariance under the choices of cutting boundaries. Three sets of cutting boundaries with the same base point are delineated, labeled with green, red and blue color. The surface T-Maps f_r, f_g and f_b with the red, green and blue cutting boundaries respectively are computed. (b), (c) and (d) show the histograms of the BC norm of the three surface map.

surfaces using beltrami holomorphic flow. Medical Image Computing and Computer-Assisted Intervention - Miccai 2010, Pt Ii, 6362, 323–330.

Lui, L.M., Wong, T.W., Zeng, W., Gu, X.F., Thompson, P.M., Chan, T.F., Yau, S.T., 2012. Optimization of surface registrations using beltrami holomorphic flow. Journal of Scientific Computing 50, 557–585.

Thompson, D., 1942. On growth and form. Cambridge University Press.

Thompson, P., Giedd, J., R.P., W., MacDonald, D., Evans, A., Toga, A., 2000. Growth patterns in the developing human brain detected using continuum-mechanical tensor mapping. Nature 404, 190–193.

Thompson, P., Lee, A., Dutton, R., Geaga, J., Hayashi, K., Eckert, M., Bellugi, U., Galaburda, A., Korenberg, J., Mills, D., Toga, A., Reiss, A., 2005. Abnormal cortical complexity and thickness profiles mapped in williams syndrome. Journal of Neuroscience 25, 4146–4158.

Tosun, D., Rettmann, M.E., Prince, J.L., 2004. Mapping techniques for aligning sulci across multiple brains. Medical Image Analysis 8, 295–309.

Vaillant, M., Qiu, A., Glaunes, J., Miller, M., 2007. Diffeomorphic metric surface mapping in subregion of the superior temporal gyrus. NeuroImage 34, 1149–1159.

Van Essen, D., Dierker, D., Snyder, A., Raichle, M., Reiss, A., Korenberg, J., 2006. Symmetry of cortical folding abnormalities in williams syndrome revealed by surface-based analyses. Journal of Neuroscience 26, 5470–5483.

Wang, Y., Chan, T., Toga, A., Thompson, P., 2009. Shape analysis with multivariate tensor-based morphometry and holomorphic differentials. IEEE 12th International Conference on Computer Vision , 2349 –2356.

Wang, Y., Zhang, J., Gutman, B., Chan, T., Becker, J., Aizenstein, H., O.L., L., Tamburo, R., Toga, A., Thompson, P., 2010. Multivariate tensor-based morphometry on surfaces: Application to mapping ventricular abnormalities in hiv/aids. NeuroImage 49, 2141–2157.

Wang, Y.L., Lui, L.M., Chan, T.F., Thompson, P.M., 2005. Optimization of brain conformal mapping with landmarks. Medical Image Computing and Computer-Assisted Intervention - Miccai 2005, Pt 2 3750, 675–683.

Wong, T., Lui, L., Thompson, P., Chan, T., 2012. Instrinic feature extraction and hippocampal surface registration using harmonic eigenmap,. SIAM Journal of Imaging Sciences 5, 746–768.

Yeo, B.T.T., Sabuncu, M.R., Vercauteren, T., Ayache, N., Fischl, B., Golland, P., 2010. Spherical demons: Fast diffeomorphic landmark-free surface registration. Ieee Transactions on Medical Imaging 29, 650–668.

Zhang, M., Li, F., He, Y., Shi, L., Wang, D., Lui, L., 2012. Tensor-based cortical surface morphometry via weighted spherical harmonic representation. Medical Image Computing and Computer Assisted Intervention (MICCAI), Part II, LNCS 7511 , 146–154.

Zhang, M., Li, F., Wang, X., Wu, Z., Xin, S., Lui, L., Shi, L., Wang, D., He, Y., 2014. Automatic registration of vestibular systems with exact landmark correspondence. Graphical Models 76, 532–541.